© 2018. Published by The Company of Biologists Ltd | Journal of Cell Science (2018) 131, jcs212233. doi:10.1242/jcs.212233

RESEARCH ARTICLE

A model suite of green algae within the Scenedesmaceae for investigating contrasting desiccation tolerance and morphology

Zoe G. Cardon[1,*], Elena L. Peredo[1], Alice C. Dohnalkova[2], Hannah L. Gershone[3] and Magdalena Bezanilla[4,5,‡]

ABSTRACT

Microscopic green algae inhabiting desert microbiotic crusts are remarkably diverse phylogenetically, and many desert lineages have independently evolved from aquatic ancestors. Here we worked with five desert and aquatic species within the family Scenedesmaceae to examine mechanisms that underlie desiccation tolerance and release of unicellular versus multicellular progeny. Live cell staining and time-lapse confocal imaging coupled with transmission electron microscopy established that the desert and aquatic species all divide by multiple (rather than binary) fission, although progeny were unicellular in three species and multicellular (joined in a sheet-like coenobium) in two. During division, Golgi complexes were localized near nuclei, and all species exhibited dynamic rotation of the daughter cell mass within the mother cell wall at cytokinesis. Differential desiccation tolerance across the five species, assessed from photosynthetic efficiency during desiccation/rehydration cycles, was accompanied by differential accumulation of intracellular reactive oxygen species (ROS) detected using a dye sensitive to intracellular ROS. Further comparative investigation will aim to understand the genetic, ultrastructural and physiological characteristics supporting unicellular versus multicellular coenobial morphology, and the ability of representatives in the Scenedesmaceae to colonize ecologically diverse, even extreme, habitats.

KEY WORDS: ROS, Photosynthesis, Multiple fission, *Scenedesmus*, *Enallax*, *Tetradesmus*

INTRODUCTION

Microscopic green algae have long been known to inhabit microbiotic crusts in arid regions world-wide (e.g. Friedmann et al., 1967; Metting, 1981). Over the last two decades, researchers combining morphological and molecular information have demonstrated that these green algae are remarkably diverse (e.g. Lewis and Lewis, 2005), belonging to at least six different green algal classes (Cardon et al., 2008). Phylogenetic analyses further revealed that, even within families and genera (e.g. Lewis and Flechtner, 2002, 2004; Fucíková et al., 2013), multiple desert lineages have evolved from aquatic ancestors independently, resulting in suites of extant related green algal species that have desert-dwelling and aquatic representatives. These related species harbor rich, natural variation that has developed in the presence of selective pressures within aquatic and desert environments.

Lewis and Flechtner (2004) described three independently evolved lineages of desert-dwelling green algae that fell within the genus *Scenedesmus: S. rotundus*, *S. deserticola* and *S. bajacalifornicus*, that were isolated from the Sevilleta desert, San Nicolas Island (off the coast of California) and Baja California, respectively. These organisms are particularly intriguing because aquatic relatives within the Scenedesmaceae have been studied for decades by a number of researchers, who focused on genetic and physiological controls over cell division by multiple fission (e.g. Bišová and Zachleder, 2014), abiotic and biotic environmental drivers of phenotypic plasticity (e.g. Trainor et al., 1976; Lampert et al., 1994), the evolution of terrestriality within green plants (e.g. Lewis and Flechtner, 2004; Lewis and Lewis, 2005; Gray et al., 2007; Cardon et al., 2008) and, more recently, biofuels development (e.g. Ho et al., 2014) and bioremediation (e.g. Suresh Kumar et al., 2015). We are building on this broad foundation, studying the three desert-derived taxa described by Lewis and Flechtner (2004) together with two sister aquatic *Scenedesmus* Meyen *sensu lato* (s.l. Scenedesmoideae) (An et al., 1999; Lewis and Flechtner, 2004; Hegewald et al., 2010) as a new model suite of organisms. Although not yet genetically tractable, the common genetic background of these five species in the Scenedesmaceae, coupled with their ecological and morphological distinctiveness, make them a promising group for comparative analyses from the variety of biological perspectives noted above.

Evolutionary relationships among our five target organisms are firmly established (Hegewald et al., 2013; Sciuto et al., 2015; Wynne and Hallan, 2015). Desert-derived *S. deserticola* and *S. bajacalifornicus* (Lewis and Flechtner, 2004) – recently renamed *Acutodesmus deserticola* and *Acutodesmus bajacalifornicus*, respectively (Hegewald et al., 2013) – fall within the same genus as aquatic *S. obliquus*, which itself was recently renamed *Tetradesmus obliquus* (Wynne and Hallan, 2015; see Materials and Methods for discussion of taxonomic nomenclature in flux). Desert-derived *S. rotundus* – recently renamed *Fletchneria rotunda* (Sciuto et al., 2015) – and aquatic *Scenedesmus costatus* – recently renamed *Enallax costatus* (Hegewald et al., 2013) – are consistently more basal within the family Scenedesmaceae, no matter which gene region was used for phylogenetic analysis (Sciuto et al., 2015).

Here, we test several hypotheses regarding cellular and physiological traits in this target suite of five ecologically and morphologically contrasting desert and aquatic taxa. Lewis and Flechtner (2004) noted that *A. bajacalifornicus*, *A. deserticola* and *F. rotunda* are unicellular, but intracellular membrane characteristics and details of division have not been previously explored. *T. obliquus* and *E. costatus* are coenobial: each mother cell produces daughter cells that are permanently physically joined side by side in a sheet-like, multicellular coenobium. Because of their contrasting

[1]Ecosystems Center, Marine Biological Laboratory, Woods Hole, MA 02543 USA. [2]Environmental Molecular Sciences Laboratory, Pacific Northwest National Laboratory, Richland, WA 99352 USA. [3]Biological Sciences and Environmental Studies Departments, Mt. Holyoke College, South Hadley, MA 01075 USA. [4]Department of Biology, University of Massachusetts, Amherst, MA 01003 USA. [5]Whitman Center, Marine Biological Laboratory, Woods Hole, MA 02543 USA. ‡Present address: Department of Biological Sciences, Dartmouth College, Hanover, NH 03755 USA.

*Author for correspondence (zcardon@mbl.edu)

Z.G.C., 0000-0001-8725-7842

Received 16 October 2017; Accepted 15 February 2018

Journal of Cell Science (2018) 131, jcs212233. doi:10.1242/jcs.212233

morphology, these five taxa provide intriguing potential as a system to study determinants of multicellularity within a common genetic background.

We first tested the hypothesis that all five taxa divide by multiple fission, as expected considering many other *Scenedesmus* sp. (Bišová and Zachleder, 2014). During multiple fission, a single mother cell commonly gives rise to more than two daughter cells during asexual reproduction. The nucleus and chloroplast in the mother cell divide into multiple copies, and cytokinesis compartmentalizes new daughter cells prior to release when the mother cell wall ruptures. Bišová and Zachleder (2014) reviewed a large body of literature focused on multiple fission in *Chlamydomonas* and *Scenedesmus quadricauda*, noting that, in *Chlamydomonas*, each of the multiple daughter cells is independent and unicellular. In *S. quadricauda*, multiple daughter cells are physically joined in a coenobium (although cytokinesis is complete). We examined whether the cells in our five target species divided by multiple fission by using overnight, time-lapse imaging of cell division and release of unicellular or coenobial daughter cells in gas-permeable polymethylsiloxane (PDMS) microfluidic chambers (Bascom et al., 2016). We then explored intracellular organellar and membrane patterns during division in more depth, using confocal microscopy for all five species and transmission electron microscopy for the three species *F. rotunda*, *A. deserticola* and *E. costatus*.

Although *A. deserticola*, *A. bajacalifornicus* and *F. rotunda* were isolated from desert microbiotic crust, DNA-based identification does not in itself demonstrate that the sequenced organisms are a permanent part of the crust community (i.e. adapted to desert conditions). Sampled organisms could be transient visitors that were, for example, deposited by chance by wind. To test for evidence of adaptation to desert conditions, Gray et al. (2007) assayed the resilience of photosynthetic activity to desiccation and rehydration in representatives from six independent desert green algal lineages and their close aquatic relatives. Among the desiccation-tolerant desert taxa analyzed by Gray et al. (2007) was *F. rotunda* (isolated by Lewis and Flechtner, 2004). After desiccation, photosynthesis in desert-derived algae rebounded more strongly and quickly upon rapid rehydration than it did in aquatic sister taxa. This rebound in photosynthetic capacity occurred in the vegetative stage of the desert-derived organisms; desiccation tolerance did not require production of a desiccation-tolerant spore that could germinate upon rehydration. The clear desiccation tolerance observed by Gray et al. (2007) supported the notion that the desert-derived algae tested by them, including *F. rotunda*, were physiologically adapted to tolerate desiccation that is common to desert habitats; they were not just coincidental, short-term visitors recently deposited on crust.

We tested the hypothesis that all three of our focal taxa isolated from deserts exhibit stronger desiccation tolerance than their two aquatic relatives – only *F. rotunda* had been tested previously. Because during desiccation and rehydration a significant source of damage can be the build-up of reactive oxygen species (ROS) within cells (Hoekstra et al., 2001; Oliver et al., 2004; Farrant and Moore, 2011), we further tested the hypothesis that the extent of desiccation tolerance across the five target taxa is mirrored by differential accumulation of cellular ROS during desiccation and rehydration.

RESULTS

Multiple fission and 3D morphology

We used confocal microscopy to examine whether the algae divided by multiple fission. Nuclei were stained with SYBR Safe; cell membranes were stained with the lipophilic dye FM4-64; and chloroplasts exhibited chlorophyll autofluorescence. We found that, in all species, the nucleus of each mother cell divided first into multiple nuclei, followed by chloroplast division and, finally, cytokinesis within the mother cell wall. Fig. 1 shows representative images for two stages of division. *T. obliquus* has undergone nuclear but not chloroplast division, and cell membranes have not yet formed around daughter cells. For the other species, Fig. 1 shows daughter cells held within the mother cell wall – having completed nuclear and chloroplast division, and cytokinesis – but not yet released from the mother cell wall. In all species, nuclear division occurred in the presence of one large chloroplast with an intact pyrenoid (e.g. *T. obliquus*, Fig. 1, pyrenoids indicated by white arrows; chlorophyll autofluorescence channel). The pyrenoid is a subcellular structure within the chloroplast where ribulose 1,5-bisphosphate carboxylase/oxygenase (RuBisCO) is concentrated; pyrenoids are commonly part of the CO_2-concentrating mechanism in green algae and appear electron dense in transmission electron microscopy (TEM). After nuclear division, the chloroplast divided, and the daughter cells were packaged by membranes delineating daughters (e.g. FM4-64 channel, all species except *T. obliquus*, Fig. 1). The pyrenoid reformed after chloroplast division and was visible in daughter cells still enclosed within the mother cell wall (Fig. 1, white arrows). Confocal *z*-stacks (Movies 1-5) and rendered volumes from them (Movies 6-10) reveal the intracellular 3D morphology.

We used TEM to examine details of intracellular structures during cell division in two desert and one aquatic species. Aquatic *E. costatus* was chosen because it is substantially larger than *T. obliquus* and, thus, easier to work with for TEM. Desert *F. rotunda* is more closely related to *E. costatus*; *A. deserticola* is more distantly related. In these three taxa, the chloroplast was easily recognizable, with internal thylakoid membranes (Fig. 2A, white arrows), starch granules and an electron-dense, prominent pyrenoid (Fig. 2A; see labels 's' and 'P', respectively). We sampled cells late in the day when we expected division to be underway. Multinucleate cells were clear in *A. deserticola* and *E. costatus* (Fig. 2A, B,E,F; nuclei labeled 'N'). At the time of sampling, *F. rotunda* had already completed cytokinesis but daughter cells were still confined within the mother cell wall (Fig. 2C,D). *E. costatus* and *A. deserticola* had undergone nuclear division but had not yet divided the chloroplast or performed cytokinesis (Fig. 2A,B and E, F, respectively). In all cases, Golgi stacks were closely associated with the nucleus (Fig. 2, blue arrowheads). The perinuclear position of these Golgi stacks was very similar to that observed with FM4-64 staining, which showed small, brightly stained membrane accumulation near the nuclei (Fig. 1, blue arrowheads). We also observed development of membrane separating daughter cells (Fig. 2E, yellow arrows), with nuclei sometimes visible and sometimes not depending on the plane of sectioning. Although the chloroplast has not divided on the right-hand side of the cell in Fig. 2E, two nuclei are visible, and membrane strands are beginning to develop between them (Fig. 2F, purple arrows). Observations such as these indicate that membrane deposition and organization began before division of chloroplasts was complete and, possibly, even before all nuclear divisions had occurred.

In all five species, we also used time-lapse imaging of chlorophyll autofluorescence to observe dynamics of division in living cells. In these taxa, a single chloroplast occupies a significant fraction of the volume of each cell. Therefore, chloroplast morphology and autofluorescence served to indicate the shape and location of the mother and then daughter cells in unstained,

Journal of Cell Science (2018) 131, jcs212233. doi:10.1242/jcs.212233

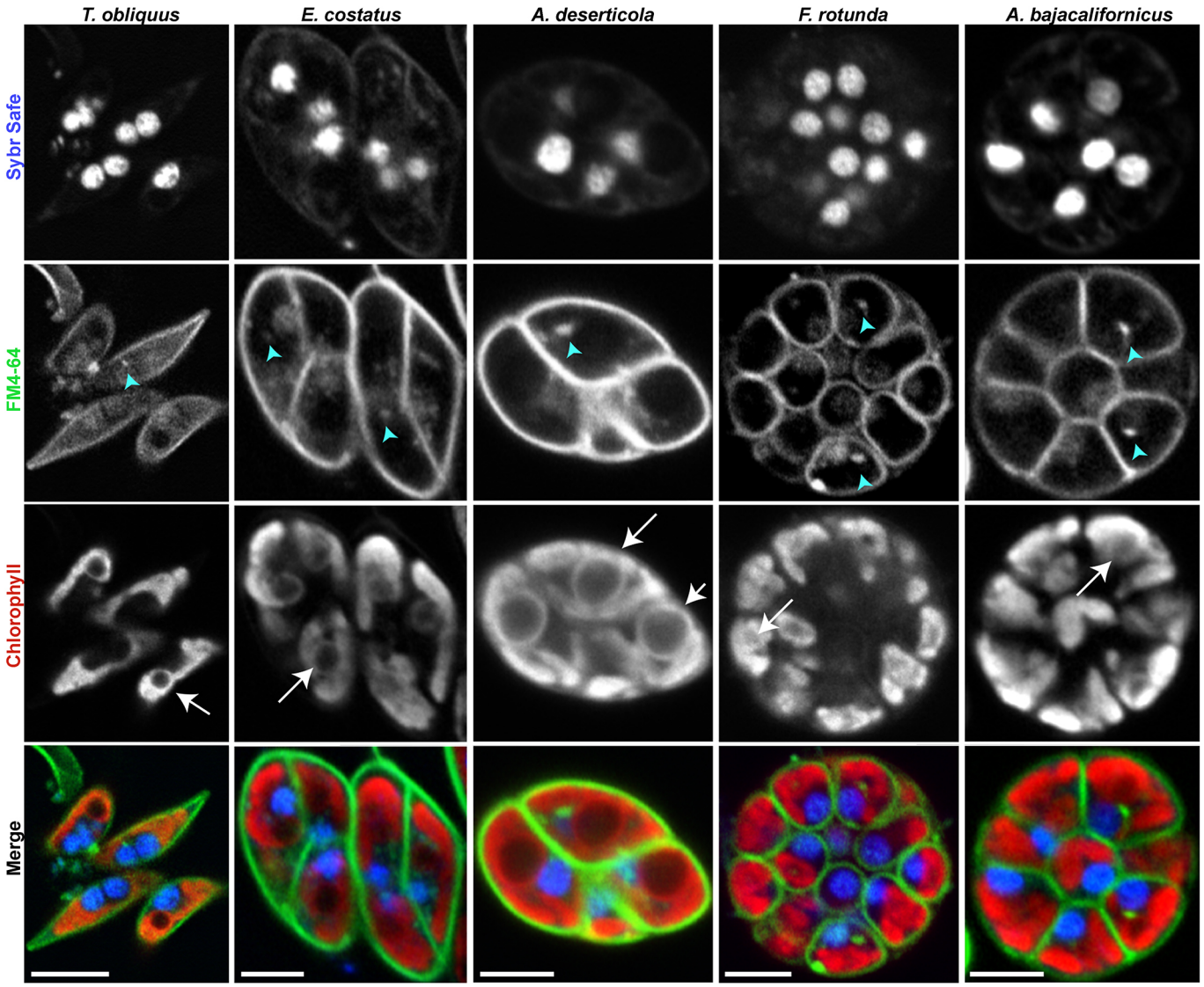

Fig. 1. Morphology and multiple fission in the five focal taxa. Single optical sections for SYBR Safe, FM4-64, and chlorophyll fluorescence are shown for each species. Merged and false-colored images show SYBR Safe (blue), FM4-64 (green), and chlorophyll (red). See text for discussion of pyrenoids (white arrows) and Golgi stacks (blue arrowheads). Scale bars: 5 µm. (See Movies 1-5 for z-stacks and Movies 6-10 for rendered volumes.) For *T. obliquus* and *E. costatus*, each mother cell within the coenobium is undergoing multiple fission and will produce a multi-celled coenobium. For *A. deserticola*, *F. rotunda*, and *A. bajacalifornicus*, the multiple daughters visible within the mother cell will be released as individual unicells.

living organisms undergoing division in PDMS chambers overnight. Interestingly, just prior to or during cytokinesis, the cell mass within the mother cell wall (as indicated by chloroplast autofluorescence) rotated as a unit. These rotations are most easily discerned in the supplementary movies (Movies 11-15) but Fig. 3 presents selected movie frames. Yellow outlines on Fig. 3 track the location of a single daughter chloroplast (or two daughters, in the case of *T. obliquus*) within a group of daughters still inside a mother cell wall. In these frames, chloroplast division has occurred, but the frame is captured just prior to or during cytokinesis. The location of the yellow-outlined daughter cell shifted as the whole cell mass reoriented within the mother cell wall (Fig. 3, Movies 11-15).

Ultimately, when the mother cell wall finally split (not shown in Fig. 3), daughter cells in *F. rotunda*, *A. deserticola* and *A. bajacalifornicus* were released as identical, independent individuals (see Fig. S1, Movie 13 for an example in *A. deserticola*). In contrast, multiple daughter cells already joined in a coenobium were released from each mother cell in *E. costatus* and *T. obliquus* coenobia. For example, Fig. S1 shows a daughter coenobium still folded up within an intact mother cell wall in *T. obliquus* at 230 min. Fifteen minutes later, at 245 min, the mother cell wall had ruptured, and the daughter coenobium had been released and had unfolded into a coenobial sheet of four joined cells (Fig. S1, Movie 11). A similar series is shown for *E. costatus* (Fig. S1, Movie 12). In contrast, four daughter cells produced within an *A. deserticola* mother cell are released as individuals at time 780 min, and only one remains in the field of view at time 805 min (Fig. S1, Movie 13).

Desiccation tolerance – photosynthetic efficiency

We used an assay of photosynthetic efficiency in the desiccated state and upon rehydration to test for desiccation tolerance in the five species. Samples from three replicate culture flasks were tested. Fig. 4 shows, for each species, the quantum yield of photosystem II (PSII) photochemistry (Φ_{PSII}) measured in the desiccated 'dry' state and at 3 min after rehydration. Φ_{PSII}, as defined by Genty et al. (1989), reflects the efficiency of electron transport per quantum absorbed by PSII.

Journal of Cell Science (2018) 131, jcs212233. doi:10.1242/jcs.212233

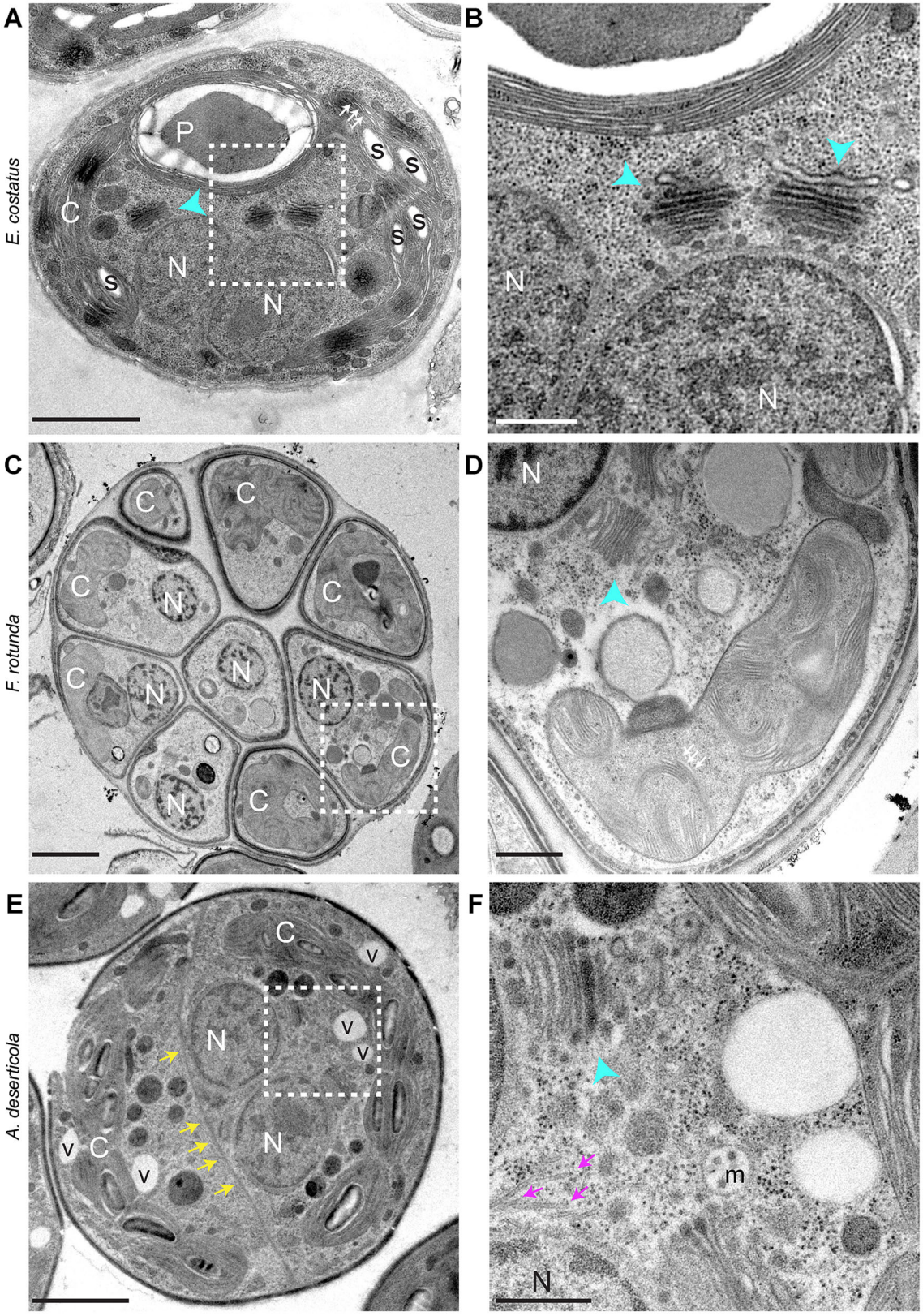

Fig. 2. Internal cell structure captured by TEM. (A) Thylakoid membranes (white arrows) within a multinucleate *E. costatus*. (B) Magnification of the boxed area in A. Golgi and associated vesicles lie near the nuclei. (C) Nine fully formed *F. rotunda* daughter cells not yet released from the mother cell wall. (D) Magnification of the boxed area in C. Golgi and associated vesicles lie near the nuclei. (E) Multi-nucleate *A. deserticola* cell with a new membrane (yellow arrows) that runs fully across the cell to the left of two nuclei and presumptive vacuoles (v). (F) Magnification of the boxed area in E. Golgi and associated vesicles lie near the nuclei, and membrane sheets (purple arrows) are visible between the two recently divided nuclei. A putative multi-vesicular body (m) is also present. For all panels, Golgi stacks are indicated by blue arrowheads. Nuclei, chloroplasts, pyrenoids, and starch granules are labeled N, C, P and s, respectively. Scale bars: 2 µm (A,C,E); 0.5 µm (B,D,F).

Journal of Cell Science (2018) 131, jcs212233. doi:10.1242/jcs.212233

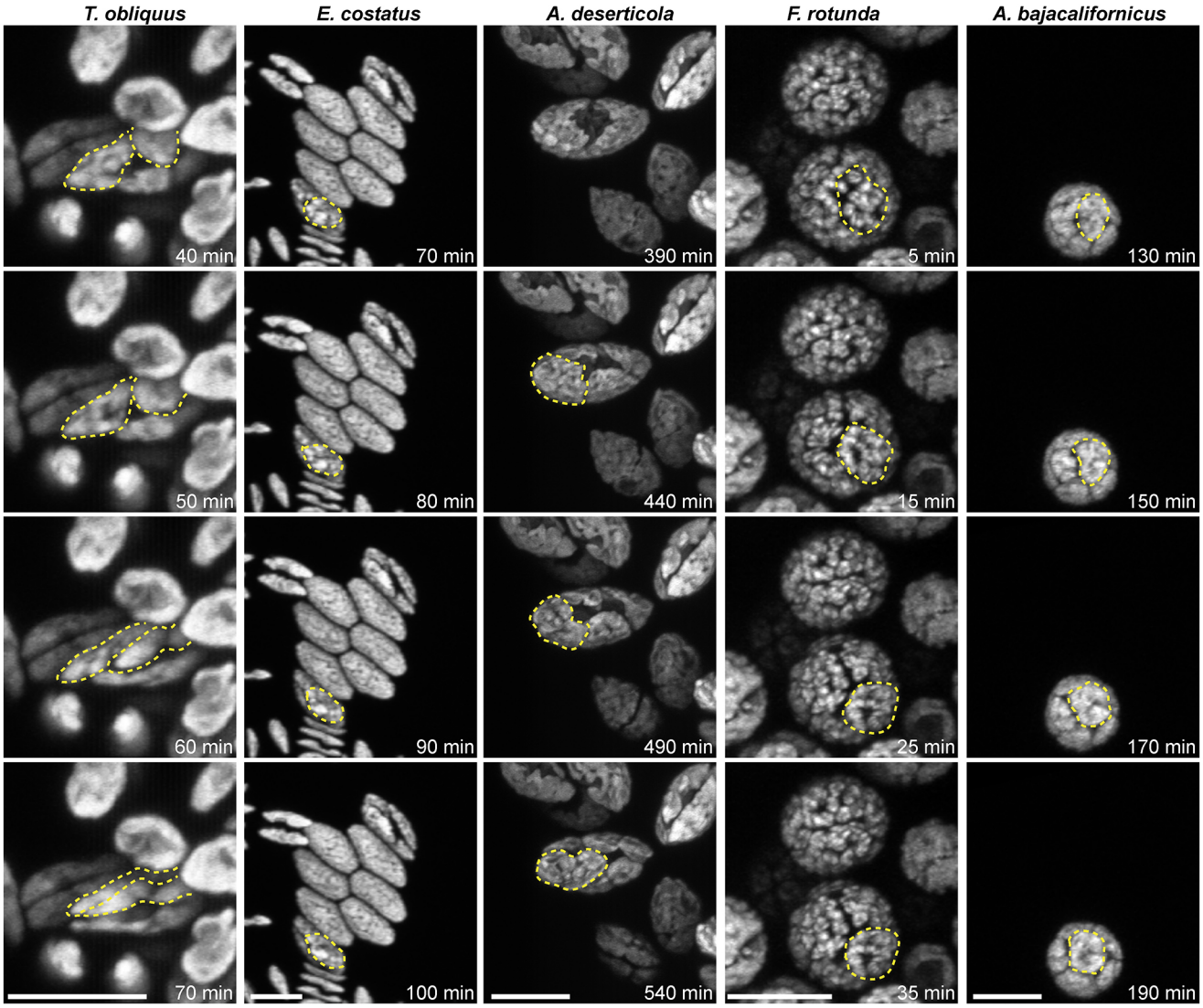

Fig. 3. Maximum intensity projections of confocal *z*-stacks during cell mass reorientation, recorded during time-lapse imaging of chlorophyll fluorescence in microfluidic chambers. Frames were extracted from Movies 11-15. For all species except *T. obliquus*, chlorophyll fluorescence from one daughter cell (as a proxy for daughter cell shape and location) is outlined with yellow dotted lines within the mother cell wall. Over the time course (indicated in each frame), the movements of the cell are traced to show the whole daughter cell mass rotating during cytokinesis. Scale bars: 10 µm. Two cells instead of one are marked in *T. obliquus*, because they are small and, thus, more difficult to distinguish. This size difference is apparent in the *E. costatus* image, where smaller coenobia of *T. obliquus* are around the periphery of the central *E. costatus* coenobium.

Φ_{PSII} is a widely used metric of photosynthetic activity and efficiency in the plant physiological and ecological literatures because it can be compared among samples (e.g. Genty et al., 1989; Maxwell and Johnson, 2000; Gray et al., 2007). All species had high Φ_{PSII} values (0.6–0.7) prior to desiccation. The Φ_{PSII} of aquatic *T. obliquus* was very low (<0.1) in both the dry and subsequent rehydrated states. *E. costatus* retained slightly higher Φ_{PSII} values immediately upon rehydration after desiccation, but values fell to Φ_{PSII} <0.1 within 3 min after rehydration and never recovered. Desert taxa had very low Φ_{PSII} when dry (tan bars, Fig. 4, *A. deserticola*, *F. rotunda* and *A. bajacalifornicus*) but, upon rehydration, Φ_{PSII} rebounded notably. The increase of Φ_{PSII} in rehydrated (relative to desiccated) algae was significantly larger in desert taxa (*A. bajacalifornicus*, *F. rotunda* and *A. deserticola*) than in aquatic taxa (*E. costatus* and *T. obliquus*) [n=3 flasks per species, tested by using generalized linear regression (GLM) with species nested within their native desert or aquatic habitat, P<0.05, Fig. 4].

Fig. S2 presents data from more-intensive testing of desiccation tolerance, from a fourth flask per species, during which algae were desiccated and rehydrated multiple times. Even after three cycles of desiccation and rehydration the Φ_{PSII} in desert species recovered upon rehydration (Fig. S2B). Fig. S2 also shows representative raw chlorophyll fluorescence data for each species that were used to quantify Φ_{PSII} during desiccation/rehydration cycles.

Desiccation tolerance – ROS

To test whether the differential desiccation tolerance detected from photosynthetic assays of the five taxa (Fig. 4) was mirrored by differential accumulation of intracellular reactive oxygen species (ROS), we used the ROS-sensitive dye $DCFH_2$-DA loaded into cells and either quantified at the population level using a Biotek Synergy plate reader, or imaged and quantified per cell on a confocal microscope. De-esterification and oxidation of $DCFH_2$-DA to highly fluorescent DCF indicates that ROS are present within cells.

Journal of Cell Science (2018) 131, jcs212233. doi:10.1242/jcs.212233

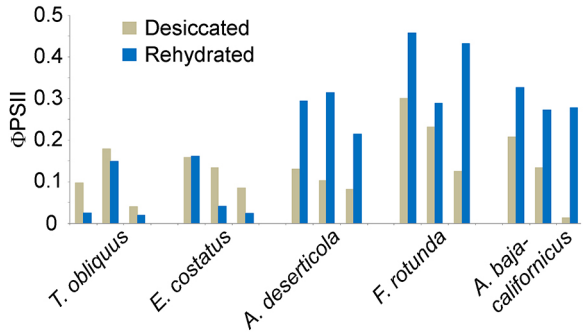

Fig. 4. Photosynthetic efficiency in the desiccated state and 3 min after rehydration, for all five taxa, as an indicator of desiccation tolerance. Quantum yield of PSII (Φ_{PSII}; samples from n=3 separate flasks per species) was assessed by measuring chlorophyll fluorescence at RT in the desiccated and then in the rehydrated state. The increase in Φ_{PSII} upon rehydration was larger in desert than in aquatic taxa (GLM test of the difference between rehydrated and desiccated states for each of the 15 flasks, species nested within desert or aquatic native habitat, P<0.05, Systat 12).

Fig. 5A shows representative confocal images of DCF fluorescence (yellow) and chlorophyll fluorescence (red) in desiccation-intolerant *T. obliquus* and in desiccation-tolerant *A. bajacalifornicus* prior to desiccation (top two panels), and after slow desiccation (bottom two panels). Images for all five species without desiccation, after slow desiccation (over ∼12 h) and after fast desiccation (in <30 min) are shown in Fig. S3. Although dye gets into all cells (see controls in Fig. S4), strong and pervasive intracellular DCF fluorescence appeared most clearly in aquatic taxa after desiccation (see yellow fluorescence, Fig. 5A, *T. obliquus*, bottom left panel).

Fig. 5B presents data from a 96-well plate-based assay of ROS in samples of algae taken from three separate culture flasks per species. DCF fluorescence from algae that were never dried (pre-desiccation) was minimal (Fig. 5B, blue bars). Fluorescence was increased from algae that were desiccated and then rehydrated with the dye solution (tan bars, Fig. 5B). This increase in DCF fluorescence (indicating ROS production), associated with the desiccation step, was significantly stronger in aquatic taxa (*E. costatus* and *T. obliquus*) than in desert taxa (*A. bajacalifornicus*, *F. rotunda* and *A. deserticola*). Samples were taken from n=3 flasks per species. The increase in DCF fluorescence caused by desiccation was significantly larger in aquatic than in desert species, as tested by GLM with species nested within desert or aquatic source habitat (P<0.05, Fig. 5B).

A more labor-intensive, in-depth exploration of DCF fluorescence at the single-cell level was conducted using confocal microscopy of samples obtained from a fourth flask per species. The intensity of yellow DCF fluorescence per cell, in all five species, is shown in Fig. S4 in box and whisker plots. Again, all five species had low DCF fluorescence per cell under fully hydrated conditions, indicating low levels of ROS (Figs S3 and S4). The desert taxa did not develop a strong increase of DCF fluorescence per cell after fast or slow desiccation (Fig. S3 and S4) unless they were actively dividing at the time of desiccation (e.g. Fig. 5A, *A. bajacalifornicus*, left bottom corner of image).

Results from several controls are also presented in Fig. S4, showing that $DCFH_2$-DA was inside cells of all species and very little fluorescence was detected when cells were not treated with $DCFH_2$-DA.

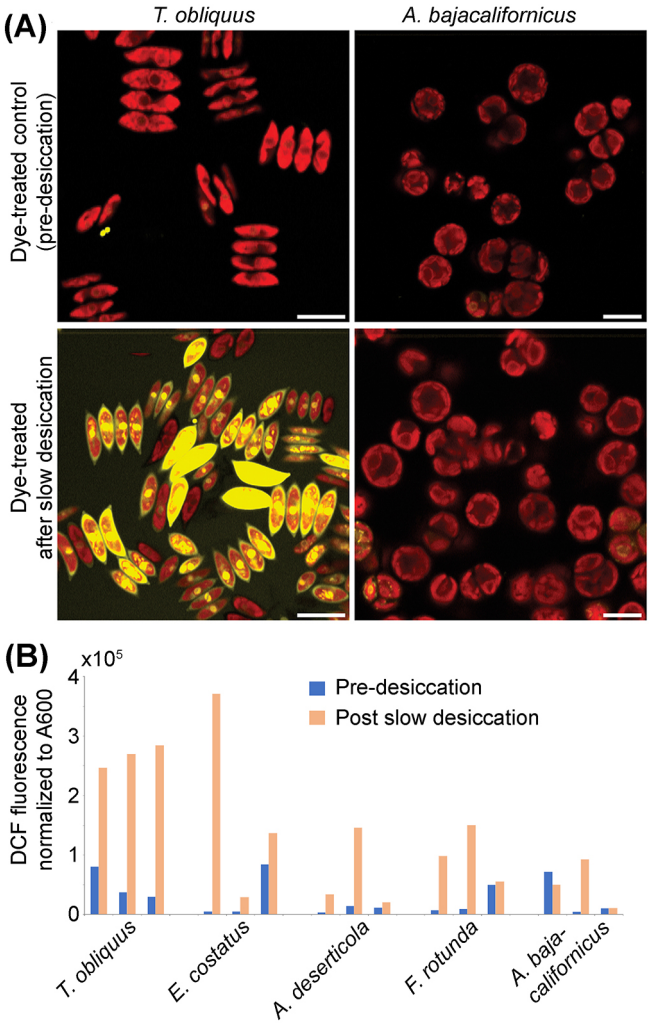

Fig. 5. DCF fluorescence spurred by ROS, prior to and after desiccation. (A) Representative confocal images of yellow DCF fluorescence (indicating the presence of ROS) and red chlorophyll fluorescence in aquatic *T. obliquus* and desert *A. bajacalifornicus*. Top images: Control cells that had never been desiccated. Bottom images: Cells after slow desiccation followed by rehydration in the solution containing $DCFH_2$-DA. Scale bars: 10 µm. (B) DCF fluorescence (normalized to A600) pre- and post-desiccation, assessed in 96-well plates using 100 µl samples of algal culture. (Samples were drawn from n=3 flasks per species. Two wells were filled per flask – one for immediate dye treatment and analysis prior to desiccation, and a second for dye treatment and analysis after desiccation.) The desiccation step resulted in higher DCF fluorescence (i.e. more ROS production) in aquatic taxa than in desert taxa (GLM test of the difference between the pre-desiccation value and post-desiccation value for each of the 15 flasks, species nested within desert or aquatic native habitat, P<0.05, Systat 12).

DISCUSSION

As a model suite of organisms, the five species within Scenedesmaceae examined here offer clear differences in desiccation tolerance (Fig. 4), as well as substantial morphological diversity (Figs 1–3, Fig. S3). To date, they are not all genetically tractable, but we are working with the U.S. Department of Energy's Joint Genome Institute (Walnut Creek, CA) to sequence the genomes of all but *A. bajacalifornicus*. Guo et al. (2013) and Chen et al. (2016) have reported some success with plasmid-based transformation of *T. obliquus*. Species within the Scenedesmaceae share many of the characteristics that supported the development of *Chlamydomonas* as a model system (Jinkerson

and Jonikas, 2015). Algae within the Scenedesmaceae and *Chlamydomonas* are micro-eukaryotes, and are easy to grow in synchronized vegetative culture (Bišová and Zachleder, 2014; Jinkerson and Jonikas, 2015). Vegetative cells are haploid, facilitating mapping of genotype and expressed phenotype. They are in the class Chlorophyceae and share a number of cellular traits with higher plants, including having chlorophyll a and b, starch as a storage compound in chloroplasts, and a cellulosic cell wall.

The very close phylogenetic relationships and shared genetic background among the five taxa targeted for study here make these algae promising organisms for identifying controls over production of unicellular versus coenobial progeny. Daughter cells are physically joined in a coenobium in aquatic taxa *E. costatus* and *T. obliquus*, but daughter cells are released as independent, unicellular individuals in desert taxa *F. rotunda*, *A. deserticola* and *A. bajacalifornicus*. While no coenobial taxa within the Scenedesmaceae have been isolated from desert microbiotic crust, the tremendous diversity of terrestrial green algae is clear (e.g. Lewis and Lewis, 2005) and a coenobial representative of the family might ultimately be isolated. Numerous publications from the 1960s to 1990s also indicate that, within some aquatic species in the family Scenedesmaceae, there can be substantial plasticity in spiny ornamentation of cells located at the ends of groups of cells joined single file into coenobia (e.g. Trainor et al., 1976; Lampert et al., 1994). Among the five taxa studied here, we observed notable differences in the numbers of daughter cells produced from each mother cell (4–8 in *T. obliquus*, *E. costatus* and *A. bajacalifornicus*; 2–4 in *A. deserticola*; and 8–32 in *F. rotunda*; see Figs 1–3, Fig. S1), but the unicellular versus coenobial fate of daughters appeared to be fixed.

Important advances in understanding of the genomic signature of multicellularity have been achieved previously by the study of the volvocine algae (Kirk, 2005), including *Chlamydomonas*. Within that clade, extant volvocine species are arrayed across a number of intermediates ranging from unicellular (independent, identical daughters as in *Chlamydonomas*) to multicellular (coenobial, functionally differentiated daughters as in *Volvox*) species (Herron and Michod, 2008). Genomic changes correlated with the degree of multicellularity (and cellular differentiation) across the clade are localized dominantly in a few main protein groups (Prochnik et al., 2010). Developmental innovations leading to multicellularity did not involve major changes in the ancestral protein repertoire but, instead, involved expansion of lineage-specific gene families and co-opting of ancestral genes into new developmental processes (Prochnik et al., 2010). A strength in this evolutionary, clade-based approach lies in the common genetic background shared by the organisms, enabling identification of genetic differences correlated with morphologically intermediate stages. Even closer phylogenetic relatedness is found among the five morphologically distinct taxa within the Scenedesmaceae introduced here, providing the opportunity for a distinct future window into determinants of coenobial multicellularity.

We took advantage of the development of gas-permeable PDMS microfluidic chambers (Bascom et al., 2016) to conduct live-cell, time-lapse imaging of cell division in these five species over many hours, from late afternoon, overnight, to morning (Fig. 3, Fig. S1, Movies 11-15). By bathing the PDMS chambers in fresh nutrient solution, we were able to maintain algae in fresh, oxygenated medium. We found they all divided as predicted – by multiple fission (Bišová and Zachleder, 2014). Results from live cells stained with SYBR and FM4-64, and from TEM, revealed that the single chloroplast in a mother cell of these species divides after nuclear division, producing multiple chloroplasts that are then each partitioned into each daughter cell during cytokinesis. Time-lapse imaging (without staining) showed that just before or during cytokinesis, the cell mass rotated within the mother cell wall (Movies 11–15), although the five taxa have cell shapes that vary from round (*F. rotunda* and *A. bajacalifornicus*) to oblate (*A. deserticola* and *E. costatus*) to very elongated (*T. obliquus*). It is possible that, in oblate and elongate species, physical forces stemming from the 3D shape of the mother cell wall drive rotation of cell mass during division and packaging into daughter cells. However, it is unclear what forces would drive the rotation of the intracellular contents in the spherical taxa *F. rotunda* and *A. bajacalifornicus*. The similar rotation in all five taxa suggests that similar mechanisms act on the cell mass during packaging of the divided chloroplasts and cytosolic components within new membranes and walls; observation of the cytoskeleton during division is clearly a next step for research.

The combination of TEM (Fig. 2) and live-cell FM4-64 staining (Fig. 1) also suggest that Golgi stacks are consistently located close to nuclei as multiple fission progresses. A small, bright FM4-64-stained structure was consistently seen in all five species near daughter cell nuclei (Fig. 1), and further investigation using TEM revealed the consistent presence of Golgi stacks near each daughter nucleus (Fig. 2). Even prior to division of the mother cell chloroplast, TEM revealed that future cell membranes were beginning to be laid down between nuclei (e.g. Fig. 2E), and vesicles are clearly seen between the Golgi stacks and the newly forming membrane. We know of no other example of integrated live-stained cell, long-term time-lapse and TEM imaging of such a suite of closely related eukaryotic microalgae of various morphologies, to examine dynamics and structural details of multiple fission at cellular and whole organism levels.

Confocal imaging of intracellular fluorescence from the ROS-sensitive dye $DCFH_2$-DA added a physiological perspective to cellular observations. The five taxa were isolated from extraordinarily different aquatic and desert environments, and our chlorophyll fluorescence-based assay of photosynthetic efficiency demonstrated that the desert-derived taxa exhibited strong desiccation tolerance (Fig. 4) – even in the face of repeated cycles of desiccation and rehydration (Fig. S2). Accompanying work in which cells were exposed to 50 µM $DCFH_2$-DA in H_2O, then imaged using a laser scanning confocal microscope, showed that cell walls were permeable to solution (Fig. S4, positive controls). Overall, the patterns in DCF fluorescence across species, observed in plate-based assays (Fig. 5B) and confocal measurements (Fig. S4), paralleled results from the chlorophyll fluorescence measurements. Desiccation tolerance assessed from Φ_{PSII} data indicated *T. obliquus*<*E. costatus*<<*A. deserticola*, *F. rotunda* and *A. bajacalifornicus* (Fig. 4). Confocal imaging showed accumulation of DCF fluorescence, particularly in the pyrenoid area, within the algal cells (e.g. in *T. obliquus* and *E. costatus*; Fig. 5A, Fig. S3), as in lichenized *Trebouxia* (Candotto Carniel et al., 2015), perhaps related to compartmentalizing oxidized mRNAs in the pyrenoid (Zhan et al., 2015). Fluorescent DCF also accumulated in the periplasmic space in the aquatic, but not the desert, taxa (Fig. S3).

Mean DCF fluorescence (indicating the presence of ROS) in aquatic *T. obliquus* and desert *A. deserticola* was stronger in slowly desiccated cells than in rapidly desiccated cells (Fig. S4, 'experimental data' boxes). This pattern was unexpected. In mosses, slow desiccation is less damaging because slow rates provide time for the synthesis of protective compounds (Cruz De Carvalho et al., 2012). We speculate that the surprising result here is a function of the daily division cycle in these rapidly growing algae.

We took cells from rapidly growing cultures in late morning, and the slow-drying treatment (over 12 h) allowed more cells to enter the division process while desiccation progressed, making them more vulnerable to damage. Fast drying in 30 min, in contrast, was likely complete prior to division being initiated in many cells, so the vulnerable dividing phase was never faced with desiccation. We base our speculation on the observation that large dividing cells e.g. in *A. deserticola*, *F. rotunda* and *A. bajacalifornicus* appear more vulnerable to build-up of ROS (Fig. 5A, Fig. S3). The photoprotective mechanism that controls the production of intracellular ROS in desert species during desiccation and rehydration remains unknown; patterns in chlorophyll fluorescence data obtained at room temperature (RT) for the three desert taxa (Fig. S2) were very similar to those observed by Veerman et al. (2007) in the desiccation-tolerant lichen *Parmelia sulcata*, which houses the green algal symbiont *Trebouxia*. Φ_{PSII} was greatly diminished because a photoprotective mechanism was engaged during desiccation (Fig. S2). Veerman et al. (2007) used time-resolved, chlorophyll fluorescence spectroscopy to show that in *Parmelia sulcata*, photoprotection resulted from the induction of an unknown mechanism dissipating energy far faster than it could be used by PSII. Slavov et al. (2013) hypothesized that a majority of this protective mechanism is spillover (sharing) of energy from the PSII antenna to PSI, although the mechanism remains unresolved.

In conclusion, these five taxa within the Scenedesmaceae are a promising group for comparative analyses targeting basic cellular and physiological questions regarding form and function of green microalgae. They share genetic background, are ecologically and morphologically distinct, and there is a rich literature describing the biology of *Scenedesmus* Meyen *sensu lato* from multiple perspectives. Well-supported ITS2, *rbc*L, *tuf*A and 18S phylogenetic trees (Sciuto et al., 2015), as well as cell wall characteristics (Hegewald et al., 2013), unite three of the species (*A. bajacalifornicus*, *A. deserticola*, *T. obliquus*) in a single genus (nomenclatural amendment pending; Wynne and Hallan, 2015). The remaining two species, *F. rotunda* and *E. costatus*, are not in the same genus; they were chosen for their contrasting ecology, morphology and basal location in the phylogeny of Scenedesmaceae. Further comparative investigation will aim to understand the genetic, ultrastructural and physiological characteristics supporting unicellular versus multicellular coenobial morphology, as well as the remarkable ability of representatives in the Scenedesmaceae to colonize ecologically diverse, even extreme, habitats.

MATERIALS AND METHODS

Taxonomic history

Each of the desert lineages used in this work is monophyletic (Lewis and Flechtner, 2004) and all have been granted species status. The nomenclature for the taxa, however, is in flux. Ongoing attempts to reorganize the family Scenedesmaceae have resulted in substantial variation in the number of genera recognized by different authors. In all papers, however – irrespective of author or genus name applied – there is no debate about the placement of *A. deserticola* within the same genus as aquatic *T. obliquus* and desert *A. bajacalifornicus*, whether that genus is labeled *Scenedesmus* (e.g. Lewis and Flechtner, 2004), *Acutodesmus* (Hegewald et al., 2013) or *Tetradesmus* (Wynne and Hallan, 2015). Currently, Algaebase and NDBI databases assign a different genus name to *T. obliquus*, *A. bajacalifornicus* and *A. deserticola*. This is not because there is argument regarding the evolutionary relatedness of the species. They are consistently placed within one genus based on multiple published biological metrics. Rather, the mismatch in genus names has resulted from a violation of nomenclatural code pointed out by Wynne and Hallan (2015) that stranded *A. bajacalifornicus* and *A. deserticola* in the *Acutodesmus* but allowed *T. obliquus* to be moved to the new genus *Tetradesmus*. This difference in genus name does not reflect the evolutionary history or relatedness of these three taxa. Close relatedness of *A. bajacalifornicus*, *A. deserticola* and *T. obliquus* is important for our work, since unicellular (*A. deserticola* and *A. bajacalifornicus*) and coenobial (*T. obliquus*) taxa are members of the same genus, no matter what that genus is currently called. (*T. obliquus* differs in 18S sequence by 8 nucleotides – 99.6% identity – from *A. bajacalifornicus*, and by 5 nucleotides – 99.7% identity – from *A. deserticola*). The other two algal species we include in our analyses (*F. rotunda* and *E. costatus*) occupy a more basal position within the subfamily Scenedemoideae. Sciuto et al. (2015) recently renamed *Scenedesmus rotundus* as *Flechtneria rotunda*, and Hegewald et al. (2013) suggest the related, basal aquatic species *Scenedesmus costatus* should revert to the genus name *Enallax*. Desert *F. rotunda* and aquatic *E. costatus* differ in 18S sequence by 23 nucleotides (98.6% identity).

Algal isolates

Below, the most-recent authority for each taxon is included within brackets, together with names considered synonymous in the NCBI database and Algaebase.

Flechtneria rotunda Sciuto & L.A. Lewis, 2015 [=*Scenedesmus rotundus* L.A. Lewis & Flechtner, 2004], isolate BCP-SEV3-VF49 from L. Lewis. GenBank accession (18S) AF513373.

Acutodesmus deserticola (L.A. Lewis & Flechtner ex E. Hegewald, C. Bock & Krienitz) E. Hegewald, C. Bock & Krienitz, 2013 [Basionym: *Scenedesmus deserticola* L.A. Lewis & V.R. Flechtner ex E. Hegewald, C. Bock & Krienitz], isolate BCP-SNI-2 from L. Lewis, GenBank accession AY510462.

Acutodesmus bajacalifornicus (L.A. Lewis & Flechtner ex E. Hegewald, C. Bock & Krienitz) E. Hegewald, C. Bock & Krienitz, 2013 [Basionym: *Scenedesmus bajacalifornicus* L.A. Lewis & Flechtner ex E. Hegewald, C. Bock & Krienitz], isolate BEA 0747B from the Banco Español de Algas, Genbank accession KY587455.

Enallax costatus (Schmidle) Pascher, 1943 [≡*Scenedesmus costatus* Schmidle, 1985; Basionym: *Scenedesmus costatus* Schmidle], isolate CCAP276-31 from the Culture Collection of Algae and Protozoa, GenBank accession HG514428.1.

Tetradesmus obliquus (Turpin) M.J. Wynne, 2016 [≡*Acutodesmus obliquus* (Turpin) Hegewald & Hanagata, 2000; ≡*Scenedesmus obliquus* (Turpin) Kuetzing; Basionym: *Achnanthes obliqua* Turpin 1828], isolate Utex 72 from the University of Texas Culture Collection, GenBank accession number X56103.

The identity of each of the unialgal cultures was confirmed by sequencing of 18S barcoding region using primers SSU1 (5′-TGGTTGATCCTGCC-AGTAG-3′) and C18G (5′-TGGCACCAGACTTGCCCT-3′); N18J (5′-CAATAACAGGTCTGTGATGCCCTTA-3′) and C18J (5′-TCTAAGGG-CATCACAGACCTGTTATTG-3′) (Lewis and Flechtner, 2002; Shoup and Lewis, 2003). Sequencing was carried out at the sequencing unit of the University of Chicago Comprehensive Cancer Center, UCCCC. The newly generated sequence for *A. bajacalifornicus* isolate BEA 0747B, strain obtained from the Banco Español de Algas, was deposited at NCBI Genbank (accession number KY587455).

Culture conditions

All species were grown in unialgal cultures. Each of the four replicate cultures of each species was started at a different time; three of four replicate flasks were 250 ml in size, one replicate flask was 50 ml in size. This difference in timing of culture start and size of culture container was intentional. As Lazic et al. (2017) (preprint) note, for clonal organisms (or cell culture lines), the idea of biological replicates is not straightforward. By starting our cultures at different times and by varying the flask size, we had cultures with slightly different histories. The statistical significance of our physiological tests of ROS production and desiccation tolerance was, therefore, more robust. All 250-ml flasks contained 100 ml of a 1:1 mix of Bold's basal medium with micronutrients (Trelease and Trelease, 1935; Bold, 1949) and Woods Hole medium (Stein, 1973). A foam stopper in the top of each 250-ml flask allowed gas exchange. The flask and stopper were fitted and autoclaved with a Pasteur pipette (with cotton plug at top) inserted through the middle of the foam stopper. Sterile solution was added to the

Journal of Cell Science (2018) 131, jcs212233. doi:10.1242/jcs.212233

flask inside a sterile hood, algae were added to solution from stock cultures; the liquid solution was bubbled with room air through the Pasteur pipette; sterility of the air was maintained by the autoclaved cotton plug. 50-ml flasks were filled in the same way but with 20 ml of solution, then loosely capped with aluminium foil and shaken at ∼100 rpm on a Gyrotory (Model G2) orbital shaker (Scientific Co. Inc., Edison, NJ), without bubbling. Cultures were maintained in a Conviron CMP4030 growth chamber (Conviron, Winnipeg, Canada) with a 12:12 L/D cycle (40 µE mixed metal halide and sodium lamps), at 25°C.

Imaging multiple fission

Cells taken from 250-ml flasks, in liquid growth medium, were incubated with a 1:1000 dilution of SYBR Safe (Life Technologies, Carlsbad, CA) for 30 min at room temperature (RT). 15 µM FM4-64 (EMD Millipore, Darmstadt, Germany) was added just prior to imaging. Cells were sandwiched between a glass slide and coverslip sealed with VALAP (1:1:1 vaseline, lanolin and paraffin) and imaged with a Nikon A1-R laser scanning confocal microscope (Nikon Instruments, Inc., Melville, NY). Samples were imaged with a resonant scanner, 60×1.49NA objective, and illuminated sequentially with 488 and 561 nm light. Emission channels were SYBR safe 450/50 band pass filter; FM4-64 525/50 band pass filter; chlorophyll fluorescence 595/50 band pass filter. 16× line scan averaging reduced acquisition noise. For time-lapse imaging, cells were loaded into gas-permeable PDMS microfluidic chambers (Bascom et al., 2016). Chlorophyll fluorescence was imaged every 5–10 min with very low laser light for up to 12 h.

TEM

High-pressure freezing (HPF) and automatic freeze substitution (AFS), followed by plastic embedding, were used to produce thin sections of respective samples of cell suspensions. Cells were left to settle in culture solution for 1 h, and 5 ml of the concentrated cell suspension was transferred into an HPF flat specimen carrier and frozen with a Leica EM PACT high-pressure freezer (Leica Microsystems, Inc., Bannockburn, IL) at a typical rate of 1700°C/s. The pods with compacted frozen cells were transferred under liquid nitrogen to the pre-cooled AFS (EM AFS; Leica), and a protocol for cell fixation, H_2O substitution by acetone and a gradual warm-up to RT was followed (Table S1). After 72 h, the samples were released from the pods, washed three times in acetone, gradually infiltrated with Spurr's low-viscosity embedding medium (Electron Microscopy Sciences, Hatfield, PA) in a series of ascending concentration (25%, 50% and 75%, followed by three washes with 100% Spurr's medium for 120 min each) and cured at 60°C for 48 h. Polymerized blocks were sectioned to 70-nm thin sections with a Leica Ultracut UCT ultramicrotome, mounted on Formvar-coated 100 mesh Cu TEM grids sputter-coated with carbon, and post-stained for 7 min with aqueous 2% uranyl acetate followed by 3 min of Reynolds' lead citrate (Reynolds, 1963) prior to TEM imaging. Samples were examined with a Tecnai T-12 TEM (FEI, Hillsboro, OR) operating at 120 kV with a LaB6 filament. Images were collected digitally with a 2×2 K Ultrascan 1000 CCD (Gatan, Pleasanton, CA).

Preparation for triplicate physiology assays – drying in 96-well plates

Assays of desiccation tolerance and intracellular ROS were conducted on separate samples of algae taken from three replicate flasks per species (two 250-ml flasks and one 100-ml flask), and deposited in 96-well plates. For ROS assays, 1 ml of culture was removed from each of the three replicate culture flasks and placed into Eppendorf tubes. Cells were allowed to settle for 10 min then 100 µl of the supernatant for each flask of each species was placed in wells of a Corning 96-well special optics low-fluorescence assay plate (Thermo Fisher Scientific), for desiccation. Another 96-well set was prepared for immediate measurements of ROS in control, never-desiccated cells. (The settling step was required to help separate very large, actively dividing cells from smaller non-dividing cells.)

For photosynthetic assays, a ∼15-ml aliquot of culture was removed mid-morning from each Ehrlenmeyer culture flask and placed into a sterile 15- or 50-ml centrifuge tube (Thermo Fisher Scientific, Waltham, MA). Algae were concentrated by allowing them to settle by gravity for 1 h in low room light (∼5 µE). Approximately 1 ml was removed from the bottom of the tube, and 100-µl aliquots of each concentrated culture sample were placed into wells of another 96-well special optics low-fluorescence assay plate.

The 96-well plates for ROS assessment in desiccated cells and for photosynthetic assays were placed in a fume hood, and the disappearance of volume of liquid in test wells around the samples was tracked over time using a micropipette. Liquid loss was homogeneous across the field of wells at ∼10 µl/h, resulting in dryness of the samples by ∼10 h.

Triplicate physiology assays – chlorophyll fluorescence

Chlorophyll fluorescence was assayed using a Walz Junior PAM chlorophyll fluorometer (Heinz Walz GmbH, Effeltrich, Germany) through the clear bottom of each sample well of the 96-well plate prepared as described above. Φ_{PSII} was calculated following equations in Genty et al. (1989). Briefly, the Walz fiber optic was positioned 1 mm below the well bottom. The fiber optic gathered and the control unit quantified chlorophyll fluorescence excited continuously by low-intensity-modulated (10 µE) white light, and also excited by saturating flashes of light (2000 µE, 600 ms duration). Φ_{PSII} was calculated as $(F_m'-F_t)/F_m'$, where F_m' is fluorescence emitted during a saturating flash, and F_t is fluorescence emitted in the presence of the modulated measuring light only. (See Fig. S2 for chlorophyll fluorescence traces with annotated F_m' and F_t, from in-depth coverslip assays described below.) The Φ_{PSII} for desiccated algae was assessed first, then 50 µl distilled H_2O was added to the well, and Φ_{PSII} assessed again 3 min after rehydration. The change in Φ_{PSII} upon rehydration was significantly larger in desert versus aquatic species, as assessed using GLM, with species nested within native habitat (desert or aquatic) (Systat 12, Richmond, CA; n=3 samples per species).

Triplicate physiology assays – ROS detection

We used the reactive oxygen species (ROS)-sensitive dye 2′,7′-dichlorodihydrofluorescin diacetate ($DCFH_2$-DA, Sigma-Aldrich, Saint Louis, MO) reconstituted with DMSO, at 50 µM concentration to assay for the presence of ROS. By using the 96-well plates prepared as described above (one containing cells that were never dried, and the other containing cells that were slow-dried, with wells tracked by flask), the DCF fluorescence (excitation 500 nm, emission 529 nm) normalized to absorbance (600 nm) from each well was assessed in a Biotek Synergy HT plate reader (Gain 100, Biotek Instruments, Winooski, VT). The difference in DCF fluorescence from never-desiccated versus desiccated-then-dye-rehydrated cells, paired by flask, was assessed using GLM, with species nested within source habitat (desert or aquatic) (Systat 12, Richmond, CA, n=3 samples per species).

Preparation for in-depth assays – rapid and slow drying of cells on coverslips

For examination of ROS by confocal microscopy, for all associated controls described in Fig. S4, and for chlorophyll fluorescence assays testing Φ_{PSII} during multiple cycles of desiccation and rehydration (Fig. S2), samples of algal were taken from only one Ehrlenmeyer flask per species, and concentrated as described above. Cell density in the concentrated sample was then adjusted to optical density 1.8 at 600 nm absorbance measured in a Biotek Synergy HT plate reader (Biotek Instruments, Winooski, VT). 40 µl drops of algal solution were then deposited onto 14 new microscope slide coverslips per species (#1.5, 18 mm×18 mm, Thermo Fisher Scientific). Seven coverslips were immediately placed in the dark to dry in a fume hood. They dried within 30 min in the flowing air, resulting in a round dot of dried algae in the center of each coverslip. (This drying was substantially faster than in the 96-well plates because the drops were unprotected on coverslips.) The remaining seven coverslips were transferred to a custom drying chamber. Light levels were less than 1 µE in the drying chamber room. Air flowed through the drying chamber, desiccating the algae slowly over 12 h. Water content of air was controlled by bubbling through warmed distilled H_2O then passing the air through a glass condenser held at 0.7°C below RT by an Isotemp 3016D water bath (Thermo Fisher Scientific). An astronomy camera (Acton PI 1 kb Versarray Cooled Camera, Princeton Instruments, Trenton, NJ, with WinView/32 software) imaged drops of algae every 30 min as they diminished in size to be sure of the slow speed of

drying (12 h to full dryness). Fast-dried and slow-dried algae were stored at RT in the dark.

In-depth assays – chlorophyll fluorescence during multiple desiccation/rehydration cycles

To assess the capacity of the various species to survive multiple cycles of desiccation and rehydration, 40 µl of algae from one flask per species were dried on three coverslips. Each coverslip, with dried algae in the center, became the bottom face of an 18 mm×18 mm×6.3 mm acrylic chamber with inlet and outlet ports for air flow (Fig. S2). The coverslip was sealed to the chamber using a thin ring of EZShape modeling clay (Polyform Products, Elk Grove Village, IL), resulting in the algae being enclosed within the chamber. Air pumped through desiccant (Drierite, Hammond Drierite Co., Xenia, OH) flowed at 1 ml/min through the chamber (over the algae), out an exit tube, and to a Licor 6262 infrared gas analyzer (Licor Inc., Lincoln, NE) connected to a Campbell Scientific CR10× datalogger (Campbell Scientific, Logan, UT) logging H_2O content of air exiting the chamber (Fig. S2).

Φ_{PSII} was assessed using the Walz Junior PAM chlorophyll fluorometer largely as in the 96-well plate experiment. The Walz fiber optic (outside the chamber) was positioned 1 mm below the coverslip, directly below the dot of algae that had been previously dried on top of the coverslip (Fig. S2A). The fiber optic gathered chlorophyll fluorescence excited continuously by low-intensity modulated (10 µE) light, and also excited by saturating flashes of light (2000 µE, 600 ms duration) applied every 3 min throughout the experiment. Φ_{PSII} was calculated as $(F_m'-F_t)/F_m'$.

At the beginning of the experiment, after one flash in the desiccated state, algae were hydrated by disconnecting the air exit tube, inserting a syringe needle through the tube port into the chamber, depositing 10 µl distilled H_2O directly onto the algae to rehydrate them, and rapidly reconnecting the air exit tube. This rehydration was designated 'Cycle 1' (Fig. S2). Saturating flashes continued to be applied every 3 min. Dry air flowed through the chamber continuously picking up H_2O and, therefore, re-drying the algae over tens of minutes. Once the Licor6262 showed the air stream was again dry, H_2O (5 µl) was injected to hydrate algae again in 'Cycle 2'. Aquatic algae showed no capacity for charge separation (no spikes of fluorescence during the saturating pulses, and therefore a quantum yield of zero, e.g. Fig. S2) after two cycles of desiccation and rehydration, so were not subjected to a third cycle. Desert algae continued responding to rehydration with increased Φ_{PSII} so were subjected to a third cycle of desiccation and rehydration and rebounded well (Fig. S2).

In-depth assay – confocal imaging of intracellular ROS

We also used $DCFH_2$-DA to assay for the presence of ROS on a per cell basis for the five species (Kalyanaraman et al. 2012), using algae deposited on coverslips as described above. Four coverslips of algae per species, were used in ROS experiments. (See Fig. S4 for a pictorial guide to the experiment.) Two coverslips had 40 µl distilled H_2O containing 50 µM $DCFH_2$-DA added to the algal cells on the coverslip: one coverslip with fast-dried cells, and one coverslip with slow-dried cells. A third coverslip held hydrated cells that had never been desiccated and to which $DCFH_2$-DA was added to bring the solution to 50 µM. The fourth coverslip held hydrated cells that had never been desiccated, and no added $DCFH_2$-DA; these algae were used to test for any autofluorescence that could interfere with the DCF signal in the assay. The four coverslips per species were then incubated 15 min, in the dark, at RT.

Cells were imaged in a confocal scanning laser microscope Axio Imager, Zeiss LSM 780 (Carl Zeiss SAS, Jena, Germany) using ×100 magnification (Plan-Apochromat 100×/1.40 oil objective) and Argon excitation laser (λ_{exc}=488 nm, 0.8% laser power, frame time 18.18 s, final image size of 85 µm^2). Cells in at least six fields of view were imaged per treatment, in multi-channel mode (DCF, λ_{em}=502-589 nm emission; chlorophyll fluorescence λ_{em}>652 nm emission). DCF fluorescence in confocal images was quantified using Image J 1.51j8 (Schneider et al., 2012; http://rsbweb.nih.gov/ij/). Cell outlines were identified from combined DCF and chlorophyll channel signals and separated when necessary by using the watershed option in ImageJ. DCF fluorescence intensity per cell was quantified as the sum of the DCF channel gray values of all the pixels in each cell divided by the number of pixels within each cell outline. The mean (±s.e.m.) number of cells contributing to each box labeled 'experimental data' in Fig. S4 was 214±32 cells (median 208 cells). The mean (±s.e.m.) number of cells contributing to each of the other boxes, from the various controls in Fig. S4, was 43±9 (median 32 cells).

All imaged cells were scored for DCF fluorescence per cell. Data from the pre-desiccation, fast desiccation and slow desiccation treatments are shown in box plots in Fig. S4. Results echo those obtained with from experiments using the Biotek plate reader but images provide the extra information that large, actively dividing cells produce ROS more readily than mature cells that are not dividing. Also, $DCFH_2$-DA is definitely entering cells of all species and ROS can be induced in all by minutes of exposure to high light. Controls illustrated there was no contamination of the DCF fluorescence signal by autofluorescence, and the extent of DCF fluorescence was not influenced by incubation time (Fig. S4).

Acknowledgements

Dr Louise Lewis (Department of Ecology and Evolutionary Biology, University of Connecticut) generously provided *F. rotunda* and *A. deserticola*. Dr John Oakey (Department of Chemical and Petroleum Engineering, University of Wyoming) generously provided PDMS microfluidic chambers. Suzanne Thomas provided expert technical assistance.

Competing interests

The authors declare no competing or financial interests.

Author contributions

Z.G.C., E.L.P. and M.B. conceived the experiments. Z.G.C., E.L.P., M.B. and H.L.G. conducted all experiments except transmission electron microscopy; A.C.D. conducted TEM. Z.G.C., E.L.P., M.B. and A.C.D. wrote the paper.

Conceptualization: Z.G.C., E.L.P., M.B.; Methodology: Z.G.C., E.L.P., A.C.D., M.B.; Validation: Z.G.C., E.L.P., M.B.; Formal analysis: Z.G.C., E.L.P., A.C.D., M.B.; Investigation: Z.G.C., E.L.P., A.C.D., H.L.G., M.B.; Resources: Z.G.C.; Data curation: E.L.P., M.B.; Writing - original draft: Z.G.C., E.L.P., A.C.D., M.B.; Writing - review & editing: Z.G.C., E.L.P., A.C.D., M.B.; Visualization: Z.G.C., E.L.P., A.C.D., M.B.; Supervision: Z.G.C., E.L.P., M.B.; Project administration: Z.G.C.; Funding acquisition: Z.G.C., M.B.

Funding

This work was supported by the National Science Foundation, Division of Integrative Organismal Systems [1355085 to Z.G.C.], an anonymous donor [to Z.G.C.], the Marine Biological Laboratory [to M.B.] and the Environmental and Molecular Sciences Laboratory (EMSL) [48938 to Z.G.C.], a Department of Energy, Office of Science User Facility sponsored by the Office of Biological and Environmental Research, located at Pacific Northwest National Laboratory.

Supplementary information

Supplementary information available online at
http://jcs.biologists.org/lookup/doi/10.1242/jcs.212233.supplemental

References

An, S. S., Friedel, T. and Hegewald, E. (1999). Phylogenetic relationships of *Scenedesmus* and *Scenedesmus*-like coccoid green algae as inferred from ITS-2 rDNA sequence comparison. *Plant Biol.* **1**, 418-428.

Bascom, C. S., Jr, Wu, S.-Z., Nelson, K., Oakey, J. and Bezanilla, M. (2016). Long-term growth of moss in microfluidic devices enables subcellular studies in development. *Plant Physiol.* **172**, 28-37.

Bišová, K. and Zachleder, V. (2014). Cell-cycle regulation in green algae dividing by multiple fission. *J. Exp. Bot.* **65**, 2585-2602.

Bold, H. C. (1949). The morphology of *Chlamydomonas chlamydogama,* sp. nov. *Bull. Torrey Bot. Club* **76**, 101-108.

Candotto Carniel, F., Zanelli, D., Bertuzzi, S. and Tretiach, M. (2015). Desiccation tolerance and lichenization: a case study with the aeroterrestrial microalga *Trebouxia* sp. (Chlorophyta). *Planta* **242**, 493.

Cardon, Z. G., Gray, D. W. and Lewis, L. A. (2008). The green algal underground: evolutionary secrets of desert cells. *Bioscience* **58**, 114.

Chen, C.-Y., Kao, A.-L., Tsai, Z.-C., Chow, T.-J., Chang, H.-Y., Zhao, X.-Q., Chen, P.-T., Su, H.-Y. and Chang, J.-S. (2016). Expression of type 2 diacylglycerol acyltransferse gene DGTT1 from *Chlamydomonas reinhardtii* enhances lipid production in *Scenedesmus obliquus*. *Biotechnol. J.* **11**, 336-344.

Cruz De Carvalho, R., Catalá, M., Marques Da Silva, J., Branquinho, C. and Barreno, E. (2012). The impact of dehydration rate on the production and cellular location of reactive oxygen species in an aquatic moss. *Ann. Bot.* **110**, 1007-1016.

Farrant, J. M. and Moore, J. P. (2011). Programming desiccation-tolerance: from plants to seeds to resurrection plants. *Curr. Opin. Plant Biol.* **14**, 340-345.

Friedmann, E. I., Lipkin, Y. and Ocampo-Paus, R. (1967). Desert algae of the Negev (Israel). *Phycologia* **7**, 185-200.
Fucíková, K., Flechtner, V. R. and Lewis, L. A. (2013). Revision of the genus *Bracteacoccus* Tereg (Chlorophyceae, Chlorophyta) based on a phylogenetic approach. *Nova Hedwigia* **96**, 15-59.
Genty, B., Briantais, J. and Baker, N. (1989). The relationship between the quantum yield of photosynthetic electron transport and quenching of chlorophyll fluorescence. *Biochim. Biophys. Acta (BBA)* **990**, 87-92.
Gray, D. W., Lewis, L. A. and Cardon, Z. G. (2007). Photosynthetic recovery following desiccation of desert green algae (Chlorophyta) and their aquatic relatives. *Plant. Cell Environ.* **30**, 1240-1255.
Guo, S.-L., Zhao, X.-Q., Tang, Y., Wan, C., Alam, M. A., Ho, S.-H., Bai, F.-W. and Chang, J.-S. (2013). Establishment of an efficient genetic transformation system in *Scenedesmus obliquus*. *J. Biotechnol.* **163**, 61-68.
Hegewald, E., Wolf, M., Keller, A., Friedl, T. and Krienitz, L. (2010). ITS2 sequence-structure phylogeny in the Scenedesmaceae with special reference to *Coelastrum* (Chlorophyta, Chlorophyceae), including the new genera *Comasiella* and *Pectinodesmus*. *Phycologia* **49**, 325-335.
Hegewald, E., Bock, C. and Krienitz, L. (2013). A phylogenetic study on Scenedesmaceae with the description of a new species of *Pectinodesmus* and the new genera *Verrucodesmus* and *Chodatodesmus* (Chlorophyta, Chlorophyceae). *Fottea* **13**, 149-164.
Herron, M. D. and Michod, R. E. (2008). Evolution of complexity in the volvocine algae: transitions in individuality through Darwin's eye. *Evolution* **62**, 436-451.
Ho, S.-H., Ye, X., Hasunuma, T., Chang, J.-S. and Kondo, A. (2014). Perspectives on engineering strategies for improving biofuel production from microalgae—A critical review. *Biotechnol. Adv.* **32**, 1448-1459.
Hoekstra, F. A., Golovina, E. A. and Buitink, J. (2001). Mechanisms of plant desiccation tolerance. *Trends Plant Sci.* **6**, 431-438.
Jinkerson, R. E. and Jonikas, M. C. (2015). Molecular techniques to interrogate and edit the *Chlamydomonas* nuclear genome. *Plant J.* **82**, 393-412.
Kalyanaraman, B., Darley-Usmar, V., Davies, K. J. A., Dennery, P. A., Forman, H. J., Grisham, M. B., Mann, G. E., Moore, K., Roberts, L. J. and Ischiropoulos, H. (2012). Measuring reactive oxygen and nitrogen species with fluorescent probes: challenges and limitations. *Free Radic. Biol. Med.* **52**, 1-6.
Kirk, D. L. (2005). A twelve-step program for evolving multicellularity and a division of labor. *BioEssays* **27**, 299-310.
Lampert, W., Rothhaupt, K. O. and Elert, E. V. (1994). Chemical induction of colony formation in a green alga (*Scenedesmus acutus*) by grazers (*Daphnia*). *Limnol. Oceanogr.* **39**, 1543-1550.
Lazic, S. E., Clarke-Williams, C. J. C. and Munafo, M. R. (2017). What exactly is 'N' in cell culture and animal experiments? *bioRxiv*.
Lewis, L. A. and Flechtner, V. R. (2002). Green algae (Chlorophyta) of desert microbiotic crusts: diversity of North American taxa. *Taxon* **51**, 443-451.
Lewis, L. A. and Flechtner, V. R. (2004). Cryptic species of *Scenedesmus* (Chlorophyta) from desert soil communities of western North America. *J. Phycol.* **40**, 1127-1137.
Lewis, L. A. and Lewis, P. O. (2005). Unearthing the molecular phylodiversity of desert soil green algae (Chlorophyta). *Syst. Biol.* **54**, 936-947.
Maxwell, K. and Johnson, G. N. (2000). Chlorophyll fluorescence- a practical guide. *J. Exp. Bot.* **51**, 659-668.
Metting, B. (1981). The systematics and ecology of soil algae. *Bot. Rev.* **47**, 195-312.
Oliver, M. J., Dowd, S. E., Zaragoza, J., Mauget, S. A. and Payton, P. R. (2004). The rehydration transcriptome of the desiccation-tolerant bryophyte *Tortula ruralis*: transcript classification and analysis. *BMC Genomics* **5**, 89.
Prochnik, S. E., Umen, J., Nedelcu, A. M., Hallmann, A., Miller, S. M., Nishii, I., Ferris, P., Kuo, A., Mitros, T., Fritz-Laylin, L. K. et al. (2010). Genomic analysis of organismal complexity in the multicellular green alga *Volvox carteri*. *Science* **329**, 223-226.
Reynolds, E. S. (1963). The use of lead citrate at high pH as an electron-opaque stain in electron microscopy. *J. Cell Biol.* **17**, 208-212.
Schneider, C. A., Rasband, W. S. and Eliceiri, K. W. (2012). NIH Image to ImageJ: 25 years of image analysis. *Nat. Methods* **9**, 671-675.
Sciuto, K., Lewis, L. A., Verleyen, E., Moro, I. and La Rocca, N. (2015). *Chodatodesmus australis* sp. nov. (Scenedesmaceae, Chlorophyta) from Antarctica, with the emended description of the genus *Chodatodesmus*, and circumscription of *Flechtneria rotunda* gen. et sp. nov. *J. Phycol.* **51**, 1172-1188.
Shoup, S. and Lewis, L. A. (2003). Polyphyletic origin of parallel basal bodies in swimming cells of chlorophycean green algae (Chlorophyta). *J. Phycol.* **796**, 789-796.
Slavov, C., Reus, M. and Holzwarth, A. R. (2013). Two different mechanisms cooperate in the desiccation-induced excited state quenching in *Parmelia* lichen. *J. Phys. Chem. B.* **117**, 11326-11336.
Stein, J. R. (1973). *Handbook of Phycological Measurements: Culture Methods and Growth Measurements*. Cambridge, UK: Cambridge University Press.
Suresh Kumar, K., Dahms, H. U., Won, E. J., Lee, J. S. and Shin, K. H. (2015). Microalgae-A promising tool for heavy metal remediation. *Ecotoxicol. Environ. Saf.* **113**, 329-352.
Trainor, F. R., Jerome, C. and Shubert, E. (1976). Morphology and nutritions of the colonial green alga *Scenedesmus*: 80 years later. *Bot. Rev.* **42**, 5-25.
Trelease, S. F. and Trelease, H. M. (1935). Changes in hydrogen-ion concentration of culture solutions containing nitrate and ammonium nitrogen. *Am. J. Bot.* **22**, 520-542.
Veerman, J., Vasil'ev, S., Paton, G. D., Ramanauskas, J. and Bruce, D. (2007). Photoprotection in the lichen *Parmelia sulcata*: The origins of desiccation-induced fluorescence quenching. *Plant Physiol.* **145**, 997-1005.
Wynne, M. J. and Hallan, J. K. (2015). Reinstatement of *Tetradesmus* G. M. Smith (Sphaeropleales, Chlorophyta). *Feddes Repert.* **126**, 83-86.
Zhan, Y., Dhaliwal, J. S., Adjibade, P., Uniacke, J., Mazroui, R. and Zerges, W. (2015). Localized control of oxidized RNA. *J. Cell Sci.* **128**, 4210-4219.